PAPER

NJC
www.rsc.org/njc

Ethylbenzene dehydrogenation to styrene in the presence of carbon dioxide over chromia-based catalysts

Xingnan Ye,[a] Weiming Hua,[a] Yinghong Yue,[a] Weilin Dai,[a] Changxi Miao,[b] Zaiku Xie[b] and Zi Gao*[a]

[a] *Laboratory of Molecular Catalysis and Innovative Materials, Department of Chemistry, Fudan University, Shanghai 200433, P. R. China. E-mail: zigao@fudan.edu.cn; Fax: +86-21-65641740; Tel: +86-21-65642792*

[b] *Shanghai Research Institute of Petrochemical Technology, Shanghai 201208, P. R. China*

Received (in Montpellier, France) 24th July 2003, Accepted 13th November 2003
First published as an Advance Article on the web 9th February 2004

The dehydrogenation of ethylbenzene to styrene in the presence of carbon dioxide over chromia-based catalysts prepared in different ways was investigated. The 25% Cr_2O_3/Al_2O_3 supported catalyst and the 20% Cr_2O_3–SiO_2 mixed oxide catalyst display the highest activities for the reaction. XRD characterization of the catalysts reveals that the activity depends on the amount of dispersed chromia species in the catalysts. A combination of XPS and TPR studies shows that both Cr^{6+} and Cr^{3+} species are present in the precalcined catalysts and the Cr^{6+} species are probably the precursors of the active sites of the catalysts with higher activity. Under the same reaction conditions, the supported chromia and chromia mixed oxide catalysts give better catalytic performance than Fe_2O_3/Al_2O_3 and V/MgO catalysts.

Introduction

Styrene is one of the most important monomers in the petrochemical industry; it is commercially produced mainly by the catalytic dehydrogenation of ethylbenzene (EB) over potassium-promoted iron oxide in the presence of an excess of overheated steam as a diluent and heat carrier.[1,2] This process is equilibrium limited and has a high energy consumption. Hence, an alternative way is still being pursued. The oxidative dehydrogenation of EB in the presence of oxygen has attracted much attention, because this reaction is free from thermodynamic constraints and can be operated at lower temperatures.[3–5] Nevertheless, a considerable decrease in styrene selectivity owing to deep oxidation of hydrocarbons to carbon oxide makes it uneconomical in view of industrial application.

EB dehydrogenation using carbon dioxide as a mild oxidant was first reported by Sato and co-workers as early as in the late 1980s.[6] Besides the necessity to solve the problem of CO_2 emission, the use of CO_2 in the reaction has aroused widespread interest later on because the energy required for this new process is estimated to be lower than that of the present commercial process and the equilibrium yield of styrene in an CO_2 atmosphere is higher than that in steam.[7] The catalyst systems giving good performance for this reaction comprise iron-oxide-based,[7–11] vanadium-oxide-based,[12–15] zirconia-based[16,17] catalysts and activated-carbon-supported chromium and cerium oxides[18] as well as calcined hydrotalcite-like compounds.[19,20] The positive roles of CO_2 in the reaction have been suggested to be the following: (1) CO_2 removes the deposited coke by the Boudouard reaction and (2) the generated hydrogen reacts with CO_2 *via* the reverse water gas shift reaction, shifting the equilibrium to the product side.[21]

In this work, ethylbenzene dehydrogenation on supported chromia and chromia mixed oxide catalysts in the presence of CO_2 was studied. The main factors affecting the activity of the catalysts are discussed.

DOI: 10.1039/b308450g

Experimental

Catalyst preparation

The γ-Al_2O_3 and SiO_2 supports used in this work have BET surface areas of 214 and 234 $m^2\ g^{-1}$, respectively. An aqueous solution of chromic nitrate was applied to the γ-Al_2O_3 and SiO_2 supports until incipient wetness, followed by drying at 383 K overnight. The supported catalysts obtained are denoted as *x*%Cr/Al and *x*%Cr/Si, where *x*% represents the weight percentage of Cr_2O_3 in the catalysts. The mixed oxide catalysts were prepared by co-precipitation and sol-gel methods. To prepare Cr–Al mixed oxide catalysts, an aqueous solution of ammonia was added dropwise under vigorous stirring to a mixed solution of $Al(NO_3)_3$ and $Cr(NO_3)_3$ until the final $pH = 8.5$ was attained. The precipitate was then filtered, washed with distilled water and dried at 383 K overnight. The Cr–Si mixed oxide catalysts were prepared by hydrolyzing TEOS (tetraethyl orthosilicate) in an aqueous ethanol solution containing a given amount of $Cr(NO_3)_3$ at 323 K and then adding a stoichiometric amount of $NH_3{\cdot}H_2O$ to the clear sol. The gel obtained was washed with distilled water and dried at 383 K overnight. The mixed oxide catalysts are labelled *x*%Cr–Al and *x*%Cr–Si, where again *x*% represents the weight percent of Cr_2O_3 in the catalysts. All the catalysts were calcined in air at 823 K for 5 h, unless otherwise noted.

For comparison, 10%Fe_2O_3/Al_2O_3 and 20%Fe_2O_3/Al_2O_3 catalysts were also prepared in the same way as the Cr/Al catalysts.

Characterization of catalysts

The BET surface areas of the supports and catalysts were measured by N_2 adsorption at 77 K on a Micromeritics ASAP 2000 instrument. X-Ray powder diffraction (XRD) patterns were recorded on a Rigaku D/MAX-IIA diffractometer with Ni-filtered CuKα radiation, operating at 30 kV and 20 mA. XRD quantitative phase analysis was carried out using pure silicon as an internal standard. The ratio of the weight of the sample to that of silicon was kept constant at 9. The peak intensity ratio $I_{Cr_2O_3}/I_{Si}$ was measured and it was assumed to be proportional to the content of crystalline Cr_2O_3. Temperature programmed reduction (TPR) experiments were carried out using a Micromeritics ASAP 2900 instrument. Samples of 200 mg of catalyst were pretreated in N_2 at 573 K for 3 h. A reduction run was then performed from 323 to 873 K at a heating rate of 10 K min^{-1} under a gas flow (40 ml min^{-1}) of hydrogen (10 vol. %) and argon (90 vol. %). X-Ray photoelectron spectroscopy (XPS) studies were performed on a Perkin–Elmer PHI-5000C ESCA system using MgKα radiation at 14 kV and 250 W. All the binding energies are referenced to the C_{1s} peak at 284.6 eV. The data were treated with an XPS peak fitting program (XPSPEAK Version 4.1 supplied by CUHK).

Activity measurement

The oxidative dehydrogenation of EB in the presence of CO_2 was carried out in a flow-type fixed-bed microreactor under atmospheric pressure. To supply the reactant, a gas mixture of N_2 and CO_2 (19:1 molar ratio, unless otherwise stated) at a flow rate of 60 ml min^{-1} was passed through a glass evaporator filled with liquid EB maintained at 273 K. The catalyst load was 100 mg and the reaction temperature was 773 K. The molar ratio of CO_2 to EB was kept constant at 19, unless otherwise stated. Prior to the reaction, the catalyst was pretreated at 773 K in N_2 for 2 h. The hydrocarbon products were analyzed with a gas chromatograph equipped with a flame ionization detector (FID).

Results

EB dehydrogenation in the presence of CO_2

The main product of EB dehydrogenation in the presence of CO_2 is styrene and the minor hydrocarbon by-products are benzene and toluene. As the reaction goes on, a slow decline in activity occurs and meanwhile the selectivity to styrene increases gradually. For all the catalysts in this work, the selectivity is higher than 98.5%.

The activities after 6 h on stream over the supported Cr/Al and Cr/Si catalysts in the presence of CO_2 as a function of chromia loading are illustrated in Fig. 1. In general, the activities of the Cr/Al catalysts are higher than those of the Cr/Si catalysts. As the Cr_2O_3 loading is increased, the conversion of EB on Cr/Al catalysts first increases and then decreases. A maximum of 59.0% conversion appears at a Cr_2O_3 loading of 25 wt. %. The selectivity to styrene at the maximum conversion is 99.0%. Over Cr/Si catalysts, the conversion of EB initially increases with Cr_2O_3 loading up to 5 wt. %, then levels off at a conversion of 22.7% and a selectivity of 99.5%.

The mixed oxide catalysts behave differently from the supported ones. The activities of the Cr–Al and Cr–Si mixed oxide catalysts after dehydrogenation for 6 h are shown in Fig. 2. Contrary to the supported catalysts, the activities of the Cr–Al catalysts are lower than those of the Cr–Si catalysts, but the selectivities to styrene on the Cr–Al catalysts are slightly higher than those on the Cr–Si catalysts. For the Cr–Al catalysts, the EB conversion increases with the Cr_2O_3 loading initially and then decreases. A maximum conversion of 45.8% and a selectivity of 99.5% are achieved at a Cr_2O_3 loading of 25 wt. %, showing that the Cr–Al mixed oxide catalysts are less active than the Cr/Al supported catalysts. The relation of the conversion of EB on Cr–Si catalysts to the Cr_2O_3 loading shows a different pattern. The activity rises more steeply at low Cr_2O_3 loading. Then, a maximum conversion of 56.0% and a selectivity of 98.8% are achieved at a Cr_2O_3 loading of 20 wt. %, that is, the Cr–Si mixed oxide catalysts are much more active than the Cr/Si supported catalysts.

Iron oxide based catalysts were reported to be effective for EB dehydrogenation in the presence of CO_2.[7–11] For comparison, the activities of 10% Fe_2O_3/Al_2O_3 and 20% Fe_2O_3/Al_2O_3 supported catalysts were tested under the same reaction conditions. The conversions of EB after 6 h on stream on 10% Fe_2O_3/Al_2O_3 and 20% Fe_2O_3/Al_2O_3 catalysts are 24.2% and 32.8%, respectively, and the selectivity to styrene on the two catalysts is 99.7%. This shows that the chromia catalysts are more active than the iron oxide catalysts for EB dehydrogenation in the presence of CO_2.

Effect of reaction conditions

The dependence of the activity and selectivity on the reaction temperature for the supported and mixed oxide catalysts is given in Table 1. The dehydrogenation activity of all the catalysts increases with reaction temperature, but the selectivity to styrene is slightly decreased. It is noteworthy that the activity rises differently with temperature on the different catalysts, implying that the apparent activation energies of the dehydrogenation reaction for these catalysts are different.

The variations of the activity and selectivity of 20%Cr/Al and 20%Cr–Si catalysts with CO_2 partial pressure are given in Table 2. The partial pressure was adjusted by changing the molar ratio of CO_2 and N_2, while the EB partial pressure, contact time factor W/F and other reaction conditions were kept unchanged. Upon introducing a small amount of CO_2

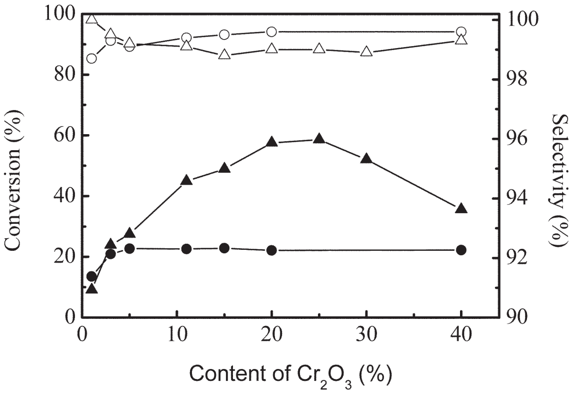

Fig. 1 Effect of Cr_2O_3 content on the conversion of EB and selectivity to styrene at 773 K after 6 h on stream for the supported catalysts. Open symbols: selectivity; filled symbols: conversion. Cr/Al catalysts: ▲, △; Cr/Si catalysts: ●, ○.

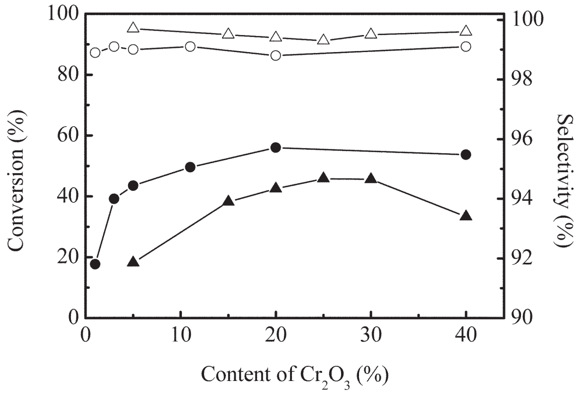

Fig. 2 Effect of Cr_2O_3 content on the conversion of EB and selectivity to styrene at 773 K after 6 h on stream for the mixed oxide catalysts. Open symbols: selectivity; filled symbols: conversion. Cr–Al catalysts: ▲, △; Cr/Si catalysts: ●, ○.

Table 1 Effect of reaction temperature on the catalytic properties of chromia catalysts[a]

Catalyst	T/K	% Conv.	% Yield	% Selectivity		
				Styrene	Benzene	Toluene
20%Cr/Al	723	26.8	26.7	99.5	0.5	–
	773	57.5	57.0	99.0	0.8	0.2
	823	76.9	75.8	98.6	0.8	0.6
20%Cr/Si	723	9.9	9.9	100	–	–
	773	22.1	22.0	99.6	0.4	–
	823	30.3	30.2	99.6	0.4	–
20%Cr–Al	723	19.0	18.9	99.4	0.6	–
	773	42.5	42.2	99.3	0.6	0.1
	823	73.4	72.6	98.8	0.8	0.4
20%Cr–Si	723	31.8	31.6	99.3	0.7	–
	773	56.0	55.3	98.8	0.7	0.5
	823	61.3	60.6	98.8	0.5	0.7

[a] Reaction conditions: 100 mg catalyst; N_2:CO_2:EB = 361:19:1; time-on-stream 6 h.

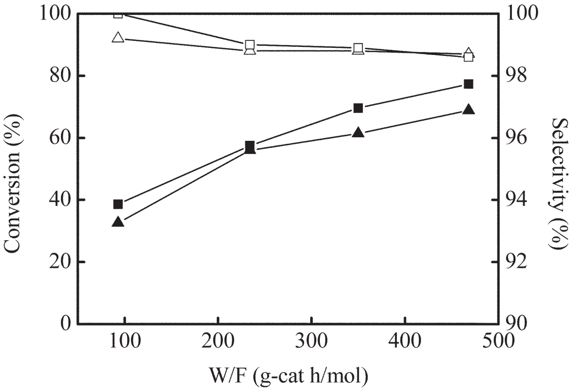

Fig. 3 Effect of W/F on the conversion of EB and selectivity to styrene at 773 K after 6 h on stream. Open symbols: selectivity; filled symbols: conversion. 20%Cr/Al: ■, □; 20%Cr–Si: ▲, △.

into the reaction, the EB conversion on both catalysts increased. The EB conversion on 20%Cr/Al catalyst remains constant at a level of 58–59% as the partial pressure of CO_2 was raised above 50 kPa, but the conversion on 20%Cr–Si catalyst drops off to 45% as the partial pressure of CO_2 is raised above 5 kPa.

The effect of the contact time factor (W/F) on the dehydrogenation of EB is illustrated in Fig. 3. The contact time factor was adjusted by changing the catalyst load while the feed flow was kept constant (N_2:CO_2:EB = 361:19:1, 60 ml min^{-1}). The EB conversion on 20%Cr/Al and 20%Cr–Si catalysts increases with an increase in W/F, but the styrene selectivity decreases gradually. In the literature,[14] the EB conversion and selectivity to styrene of the V/MgO catalyst in the presence of CO_2 (CO_2/EB = 45) at 773 K and W/F = 70 (g cat) h mol^{-1} after 1 h on stream were reported to be 17.2% and 92.2%, respectively. The results in Fig. 3 show that 20%Cr/Al and 20%Cr–Si catalysts are probably more active and selective than the supported vanadium oxide catalyst under the same reaction conditions.

Dispersion of Cr_2O_3 on the catalysts

XRD patterns of some representative Al_2O_3 and SiO_2 supported chromia catalysts calcined at 823 K are shown in Figs. 4 and 5. For the Cr/Al series of catalysts, no distinct diffraction peaks corresponding to Cr_2O_3 crystals appear until a 25 wt. % Cr_2O_3 loading is reached, demonstrating that chromia is readily dispersed on the Al_2O_3 support. In contrast, diffraction peaks of crystalline Cr_2O_3 were observed on the Cr/Si catalysts with a Cr_2O_3 loading as low as 3 wt. %. Increasing the Cr_2O_3 loading on the SiO_2 support results in an increase of the diffraction intensity. The peak intensities of the reflections (104) for Cr_2O_3 in Cr/Al catalysts and (116) for Cr_2O_3 in Cr/Si catalysts were measured and compared with those of the silicon standard. The quantitative phase analysis data are depicted in Fig. 6, showing that the dispersion thresholds of Cr_2O_3 on γ-Al_2O_3 and SiO_2 are 21.3 and 1.2 wt. %, respectively. According to the crystallographic data of Cr_2O_3, one monolayer of Cr_2O_3 is equivalent to *ca.* 10 atoms of Cr per 1 nm^2 of the support.[22] Therefore, the formation of a monolayer of Cr_2O_3 on the surface of the γ-Al_2O_3 and SiO_2 supports corresponds to Cr_2O_3 loadings of *ca.* 21 and 23 wt. %, respectively. The fact that the dispersion threshold of Cr_2O_3 on γ-Al_2O_3 detected by the XRD method is close to the estimated monolayer surface coverage implies that chromia is probably dispersed as a monolayer on the γ-Al_2O_3 support when its loading is lower than the threshold, due to the strong interactions between chromia and the Al_2O_3 support. On the other hand, the dispersion threshold of Cr_2O_3 on SiO_2 is much smaller than the theoretical monolayer surface coverage, indicating that chromia tends to aggregate and form microcrystals rather than to disperse on the surface of the SiO_2 support. The above results are consistent with those found by Wang *et al.*[23] on similar supported chromia catalysts.

The XRD patterns of the Cr–Al and Cr–Si mixed oxide catalysts calcined at 823 K are shown in Figs. 7 and 8. The Cr–Al and Cr–Si mixed oxide catalysts do not display distinct diffraction peaks due to crystalline Cr_2O_3 until the content of Cr_2O_3 reaches 30 and 20 wt. %, respectively, indicating that

Table 2 Effect of CO_2 partial pressure on the catalytic properties of chromia catalysts[a]

Catalyst	$P(CO_2)$/kPa	% Conv.	% Yield	% Selectivity		
				Styrene	Benzene	Toluene
20%Cr/Al	0	48.9	48.3	98.9	1.0	0.1
	5	57.5	57.0	99.0	0.8	0.2
	51	59.0	58.3	98.9	0.9	0.2
	99	58.3	57.7	98.9	0.9	0.2
20%Cr–Si	0	51.7	51.3	99.1	0.6	0.3
	5	56.0	55.3	98.8	0.7	0.5
	51	44.9	44.3	98.8	0.7	0.5
	99	45	44.4	98.5	1.0	0.5

[a] Reaction conditions: 100 mg catalyst; EB feed rate 0.42 mmol h^{-1}; 773 K; time-on-stream 6 h.

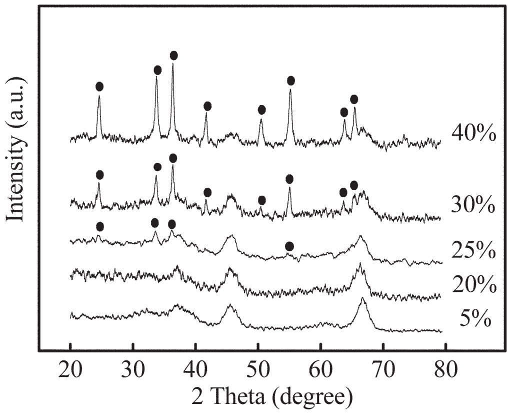

Fig. 4 XRD patterns of a series of Cr/Al catalysts calcined at 823 K; (●) crystalline Cr_2O_3.

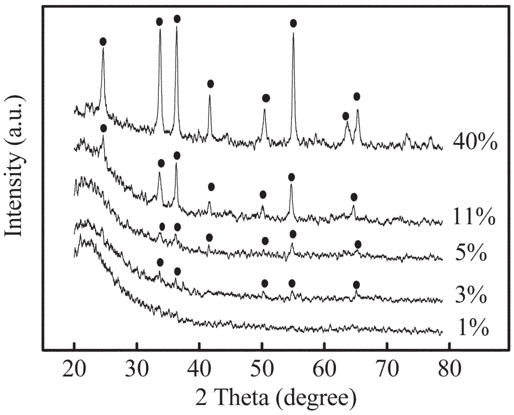

Fig. 5 XRD patterns of a series of Cr/Si catalysts calcined at 823 K; (●) crystalline Cr_2O_3.

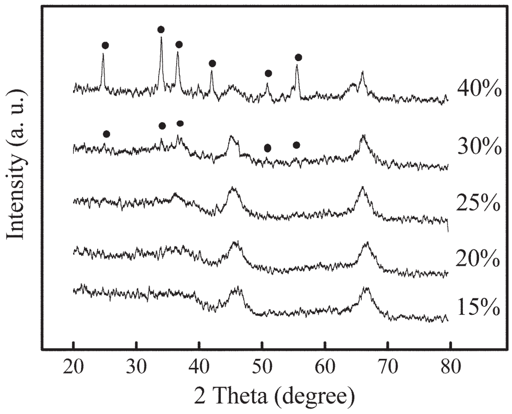

Fig. 7 XRD patterns of a series of Cr–Al catalysts calcined at 823 K; (●) crystalline Cr_2O_3.

aggregation of Cr_2O_3 crystallites in the mixed oxide catalysts begins at Cr_2O_3 contents higher than those of the supported catalysts. The discrepancy is brought about by the different distribution patterns of chromia in the catalysts. For the mixed oxide catalysts, chromia is certainly distributed not only on the surface but also in the bulk of the catalysts.

The BET surface areas of the supported and mixed oxide catalysts calcined at 823 K are listed in Table 3. For the Cr/Al and Cr/Si supported catalysts, the surface area decreases gradually with an increase in Cr_2O_3 loading, which is common for these supported catalysts.[24] The Cr–Al and Cr–Si mixed oxide catalysts have larger surface areas than the analogous supported catalysts and the surface areas for these catalysts first rise and then fall with chromia content.

XPS and TPR studies

The XPS spectra of some of the studied catalysts were recorded. The spectra were deconvoluted into two bands at about 576 and 579 eV assigned to Cr^{3+} and Cr^{6+} ions, respectively.[25] The fraction of Cr^{6+} ions in the total amount of chromium calculated from the relative intensities of the two bands is listed in Table 4, showing that a considerable amount of Cr^{6+} species is present on the surface of the catalysts after calcination at 823 K in air. The atomic ratios between Cr and Al(Si) calculated from the Cr(2p) and Al(2p) or Si(2p) bands are also given in Table 4. The Cr/Al(Si) ratio increases with the Cr loading of the supported catalysts and, as expected, it is smaller for mixed oxide catalysts with the same Cr content.

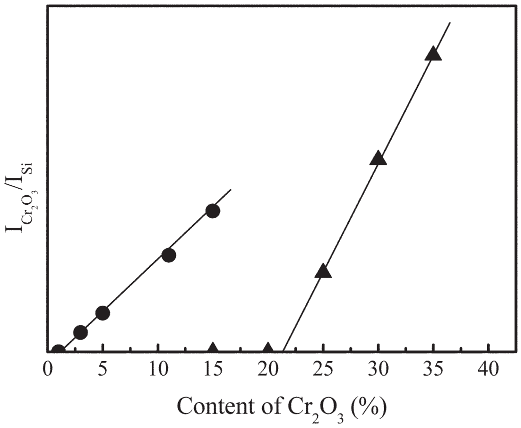

Fig. 6 Dispersion thresholds of Cr_2O_3 on γ-Al_2O_3 and SiO_2 supports; (▲) γ-Al_2O_3, (●) SiO_2.

Partial reduction of the Cr^{6+} species is observed in the 20%Cr/Al catalyst after reaction for 6 h.

The TPR profiles of the catalysts are depicted in Fig. 9. For bulk Cr_2O_3, only one weak reduction peak appears in the profile at 538 K, corresponding to the reduction of Cr^{6+} in the oxide.[26] There is also one reduction peak on the TPR profiles of 5%Cr/Al, 5%Cr–Al and 5%Cr–Si catalysts, but the peak temperature is shifted towards higher temperatures, suggesting that the oxygen is more strongly bound in the dispersed chromia on the catalysts.[27] Both the low temperature (peak I) and high temperature (peak II) peaks are observed in the profile of the 5%Cr/Si catalyst, showing that large crystals of chromia exist on the catalyst as well as the dispersed oxide. This is consistent with the result of the XRD measurement. For all the supported and mixed oxide catalysts containing 20 wt. % Cr_2O_3, a small peak or a shoulder peak around 545 K is observed along with the high temperature reduction peak, implying that some undispersed crystalline chromia is present in these catalysts. Since the Cr loadings of our catalysts are high, it can be assumed that the Cr^{6+} in the catalysts is mostly reduced to Cr^{3+}.[28,29] The TPR data as well as the amount of Cr^{6+} in the catalysts calculated from the total H_2 consumption are listed in Table 5. The concentration of Cr^{6+} varies with the type of catalyst and the total amount of chromia in the catalyst.

Discussion

The variation of EB dehydrogenation activity with Cr loading in the presence of CO_2 in Fig. 1 reveals that the dispersed chromia phase on the supports is crucial for the reaction.

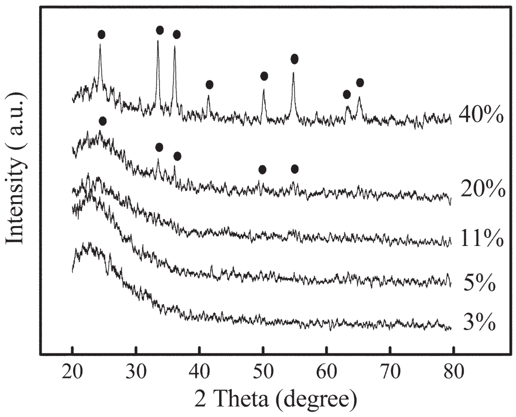

Fig. 8 XRD patterns of a series of Cr–Si catalysts calcined at 823 K; (●) crystalline Cr_2O_3.

Table 3 BET surface areas of the catalysts calcined at 823 K

	Surface area/m^2 g^{-1}			
Cr_2O_3 content/wt. %	Cr/Al	Cr/Si	Cr–Al	Cr–Si
0	214	234	–	–
5	203	170	298	421
11	198	164	310	447
20	173	148	247	446
30	144	124	200	–
40	124	107	151	349

The catalytic activity of the Cr/Al supported catalysts exhibits a maximum at a Cr_2O_3 loading of 25 wt. %, corresponding approximately to monolayer surface coverage of Cr_2O_3 on the γ-Al_2O_3 support, whereas the activity of the Cr/Si catalysts levels off at a much lower value with a Cr_2O_3 loading far below monolayer surface coverage. The difference in activity between the two types of supported catalysts arises from the low dispersion of chromia on the surface of the SiO_2 support. Chromia is hardly spread over the support surface after calcination. This particular behavior of SiO_2 limits its use as a support for EB dehydrogenation catalyst.

The variation of catalytic activity with Cr loading on mixed oxide catalysts in Fig. 2 is significantly different from that on supported catalysts. For both Cr–Al and Cr–Si mixed oxide catalysts, the activity initially increases with Cr_2O_3 loading and then decreases. The maximum activity of Cr–Al and Cr–Si catalysts appears at Cr_2O_3 loadings of 25 and 20 wt. %, respectively. XRD patterns of the Cr–Al and Cr–Si catalysts in Figs. 7 and 8 show that the aggregation of large Cr_2O_3 crystallites in Cr–Al and Cr–Si catalysts begins at Cr_2O_3 loadings of 30 and 20 wt. %, respectively. These results further confirm that the dispersity of chromia in the mixed oxide catalysts is also related to the dehydrogenation reactivity. The Cr–Si mixed oxide catalyst gives better performance for the reaction than the Cr/Si supported catalyst with the same Cr content, since chromia is more homogeneously distributed in the mixed oxide catalyst. The Cr–Si mixed oxide catalyst gives a better performance for the reaction than the Cr/Si supported catalyst with the same Cr content. In particular, the Cr–Si mixed oxide catalysts with low Cr content display exceedingly high activity in comparison to all the other catalysts. This is probably due to the more homogeneous distribution of chromia species in the catalysts, resulting from the sol-gel preparation method.

The XPS and TPR measurements have shown the coexistence of Cr^{3+} and Cr^{6+} species in the catalysts before the reaction. In previous literature,[30,31] the *n*-butane dehydrogenation activity of Cr_2O_3/Al_2O_3 catalysts increased parallel to the initial amount of Cr^{6+} in the catalysts. The high-oxidation-state Cr species were suggested to be the precursors of the active sites of the catalysts.

Table 4 XPS data for the catalysts

	B.E. Cr($2p_{3/2}$)/eV			
Catalyst	Cr^{3+}	Cr^{6+}	Cr^{6+}/Cr	Cr/Al(Si)
5%Cr/Al	576.8	579.1	0.42	0.13
5%Cr/Si	576.4	578.8	0.28	0.10
20%Cr/Al	576.7	579.3	0.36	0.35
20%Cr/Al[a]	576.7	579.3	0.18	0.31
20%Cr–Al	576.8	579.3	0.31	0.26
20%Cr–Si	576.1	578.6	0.48	0.15

[a] After reaction at 773 K for 6 h.

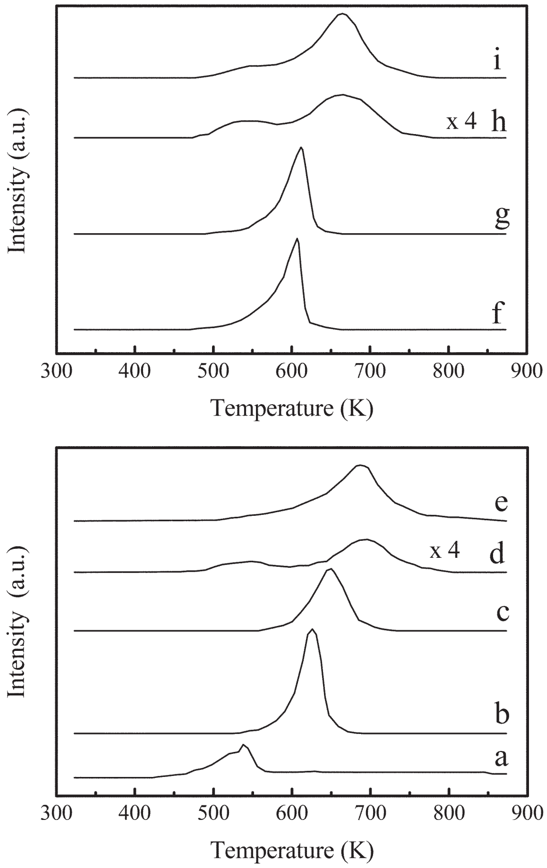

Fig. 9 TPR profiles of some samples: (a) bulk Cr_2O_3; (b) 5%Cr/Al; (c) 5%Cr–Al; (d) 5%Cr/Si; (e) 5%Cr–Si; (f) 20%Cr/Al; (g) 20%Cr–Al; (h) 20%Cr/Si; (i) 20%Cr–Si.

The EB conversion of our catalysts is plotted against the amount of Cr^{6+} determined by the TPR method in Fig. 10. The correlation is not as linear as that shown in the literature[31] due to the diversity of the catalysts studied in this work, but the positive effect of the Cr^{6+} species on the reaction is evident, suggesting that the Cr^{6+} species are probably the precursors of the active sites, whch have a higher activity for the EB conversion as well.[30,31] Besides the Cr^{6+} content, there are probably other minor factors, such as the difference in specific surface area among the catalysts (see Table 3), the difference in distribution of the Cr species between the supported and the mixed oxide catalysts and the difference in interactions between Cr–Al and Cr–Si in the catalysts, that may also affect the activity of the catalysts.

It is noteworthy that the reducibility of the Cr^{6+} species in the Cr/Si and Cr–Si catalysts represented by the reduction peak temperature (see Table 5) is lower than that in Cr/Al and Cr–Al catalysts, indicating that the oxygen is more strongly bound in the former catalysts. However, this difference in reducibility does not exert much influence on the EB dehydrogenation activity of the catalysts. This is probably because the dehydrogenation reaction is carried out at temperatures much high than the reduction temperature of the chromia species.

In the presence of an appropriate amount of CO_2, the conversion of EB on the catalysts is increased, whereas the selectivity to styrene is almost unchanged. The enhancement in activity can be attributed to the oxidative dehydrogenation of ethylbenzene by the oxygen species originating from CO_2.[9,16] An excess of CO_2 may somewhat reduce the activity of the catalysts. The reason for this behavior may be related to the decreased adsorption of EB in the presence of large amounts of CO_2.

Table 5 TPR data for the catalysts

	Peak I		Peak II			
Catalyst	T/K	H_2/mmol (g cat)$^{-1}$	T/K	H_2/mmol (g cat)$^{-1}$	Total H_2/mmol (g cat)$^{-1}$	Cr^{6+}/mmol (g cat)$^{-1}$
5%Cr/Al	–	–	626	0.564	0.564	0.376
5%Cr/Si	548	0.050	696	0.185	0.235	0.157
5%Cr–Al	–	–	650	0.489	0.489	0.326
5%Cr–Si	–	–	687	0.549	0.549	0.366
20%Cr/Al	–	–	607sh[a]	0.780	0.780	0.520
20%Cr/Si	547	0.074	666	0.248	0.322	0.215
20%Cr–Al	–	–	612sh	0.743	0.743	0.495

[a] sh: with shoulder peak at lower temperature.

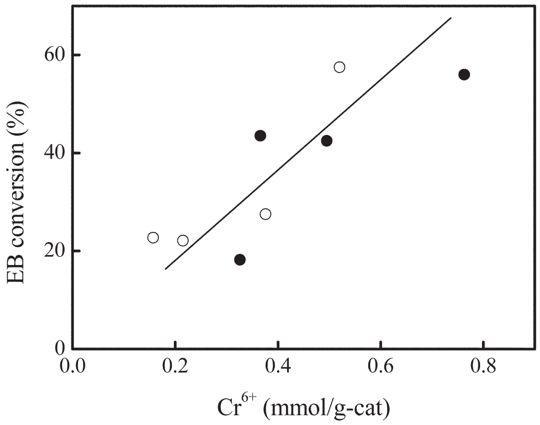

Fig. 10 The correlation between activity and the amount of Cr^{6+} in the catalysts: (○) supported catalysts; (●) mixed oxide catalysts.

Conclusions

The catalytic activities and selectivities of supported chromia catalysts and chromia mixed oxide catalysts for EB dehydrogenation in the presence of CO_2 were compared. The selectivity to styrene of all the catalysts is above 98.5%, but the activity of the catalysts differs from one to another. The γ-Al_2O_3 supported chromia catalyst is much more active than the SiO_2 supported chromia catalyst, whereas the chromia–silica mixed oxide catalyst is more active than the chromia–alumia mixed oxide catalyst. The EB dehydrogenation activity increases with Cr_2O_3 loading up to a value slightly higher than the dispersion threshold of Cr_2O_3 on the supports determined by XRD, that is 25 and 5 wt. % for the Cr/Al and Cr/Si supported catalysts, respectively. On the other hand, the maximum activity of the Cr–Al and Cr–Si mixed oxide catalysts appears at a Cr_2O_3 content of 25 and 20 wt. %, respectively, just before microcrystals of Cr_2O_3 are detected in the XRD pattern of the catalyst. The above results suggest that the dispersed chromia species in the catalysts are more active than crystalline Cr_2O_3 for the reaction.

XPS and TPR studies reveal that both Cr^{6+} and Cr^{3+} are present in the catalysts after calcination in air. A correlation between the activity and the amount of Cr^{6+} species in the fresh catalyst is observed, although discrepancies are significant in some cases, indicating the presence of other possible influencing factors. The high-oxidation-state Cr species are probably the precursors of the active sites, which have a higher activity for the dehydrogenation reaction.

Acknowledgements

The work was supported by the Chinese Major State Basic Research Development Program (Grant 2000077507) and Shanghai Research Institute of Petrochemical Technology.

References

1 E. H. Lee, *Catal. Rev.*, 1973, **8**, 285.
2 W. D. Mross, *Catal. Rev. Sci. Eng.*, 1983, **25**, 591.
3 F. Cavani and F. Trifiro, *Appl. Catal., A*, 1995, **133**, 219.
4 W. S. Chang, Y. Z. Chen and B. L. Yang, *Appl. Catal., A*, 1995, **124**, 221.
5 W. Oganowski, J. Hanuza and L. Kepinski, *Appl. Catal., A*, 1998, **171**, 145.
6 S. Sato, M. Ohhara, T. Sodesawa and F. Nozaki, *Appl. Catal.*, 1988, **37**, 207.
7 N. Mimura, I. Takahara, M. Saito, T. Hattori, K. Ohkuma and M. Ando, *Catal. Today*, 1998, **45**, 61.
8 M. Sugino, H. Shimada, T. Turuda, H. Miura, N. Ikenaga and T. Suzuki, *Appl. Catal., A*, 1995, **121**, 125.
9 T. Badstube, H. Papp, P. Kustrowski and R. Dziembaj, *Catal. Lett.*, 1998, **55**, 169.
10 N. Mimura and M. Saito, *Catal. Lett.*, 1999, **58**, 59.
11 T. Badstube, H. Papp, R. Dziembaj and P. Kustrowski, *Appl. Catal., A*, 2000, **204**, 153.
12 Y. Sakurai, T. Suzaki, N. Ikenaga and T. Suzuki, *Appl. Catal., A*, 2000, **192**, 281.
13 Y. Sakurai, T. Suzaki, K. Nakagawa, N. Ikenaga, H. Aota and T. Suzuki, *Chem. Lett.*, 2000, 526.
14 Y. Sakurai, T. Suzaki, K. Nakagawa, N. Ikenaga, H. Aota and T. Suzuki, *J. Catal.*, 2002, **209**, 16.
15 V. P. Vislovskiy, J.-S. Chang, M.-S. Park and S.-E. Park, *Catal. Commun.*, 2002, **3**, 227.
16 J.-N. Park, J. Noh, J.-S. Chang and S.-E. Park, *Catal. Lett.*, 2000, **65**, 75.
17 J. Noh, J.-S. Chang, J.-N. Park, K. Y. Lee and S.-E. Park, *Appl. Organometal. Chem.*, 2000, **14**, 815.
18 N. Ikenaga, T. Tsuruda, K. Senma, T. Yamaguchi, Y. Sakurai and T. Suzuki, *Ind. Eng. Chem. Res.*, 2000, **39**, 1228.
19 N. Mimura, I. Takahara, M. Saito, Y. Sasaki and K. Murata, *Catal. Lett.*, 2002, **78**, 125.
20 P. Kustrowski, A. Rafalska-Lasocha, D. Majda, D. Tomaszewska and R. Dziembaj, *Solid State Ionics*, 2001, **141–142**, 237.
21 O. V. Krylov, A. K. Mamedov and S. R. Mirzabekova, *Ind. Eng. Chem. Res.*, 1995, **34**, 474.
22 B. Grzybowska, J. Sloczynski, R. Grabowski, K. Wcislo, A. Kozlowska, J. Stoch and J. Zielinski, *J. Catal.*, 1998, **178**, 687.
23 S. Wang, K. Murata, T. Hayakawa, S. Hamakawa and K. Suzuki, *Appl. Catal., A*, 2000, **196**, 1.
24 M. Cherian, M. S. Rao, A. M. Hirt, I. E. Wachs and G. Deo, *J. Catal.*, 2002, **211**, 482.
25 W. Grunert, E. S. Shpiro, R. Feldhaus, K. Auders, G. V. Autoshin and K. M. Minachev, *J. Catal.*, 1986, **100**, 138.
26 M. Cherian, M. S. Rao, W. T. Yang, J. M. Jehng, A. M. Hirt and G. Deo, *Appl. Catal., A*, 2002, **233**, 21.
27 C. M. Pradier, F. Rodrigues, P. Marcus, M. V. Landau, M. L. Kaliya, A. Gutman and M. Herskowitz, *Appl. Catal., B*, 2000, **27**, 73.
28 A. Zecchina, E. Garrone, G. Ghiotti, C. Morterra and E. Borello, *J. Phys. Chem.*, 1975, **79**, 966.
29 A. Hakuli, M. E. Harlin, L. B. Backman and A. O. Krause, *J. Catal.*, 1999, **184**, 349.
30 S. Rossi, M. Casaletto, G. Ferraris, A. Cimino and G. Minelli, *Appl. Catal., A*, 1998, **167**, 257.
31 A. Hakuli, A. Kytokivi, A. O. Krause and T. Suntola, *J. Catal.*, 1996, **161**, 393.